Available online at www.sciencedirect.com
ScienceDirect
Carbohydrate Research 343 (2008) 1091–1098
Carbohydrate RESEARCH

Conformational free energy maps for globobiose (α-D-Gal*p*-(1→4)-β-D-Gal*p*) in implicit and explict aqueous solution

Michelle M. Kuttel*

Department of Computer Science, University of Cape Town, Cape Town, South Africa

Received 8 November 2007; received in revised form 20 December 2007; accepted 7 January 2008
Available online 5 February 2008

Abstract—Four Ramachandran maps of the conformational potential of mean force (PMF) for the galactose disaccharide globobiose (α-D-Gal*p*-(1→4)-β-D-Gal*p*) were calculated in vacuum, explicit water, with a simple high dielectric constant and a distance-dependent dielectric coefficient, respectively. This simple model of the galactan α-(1→4)-linkage is shown to be conformationally restricted, with only a small range of *syn*-ϕ/*syn*-ψ conformations predominating at standard temperature and pressure. This has implications for the preferred conformation and chain dynamics of α-galactosides. In addition, comparison of the relevant PMF surfaces reveals the substitution of a high dielectric constant for explicit water solution to be a valid approximation for reproducing the minimum energy conformation of this glycosidic linkage.

Keywords: Globobiose; Digalactoside; Free energy; Disaccharide; Potential of mean force; Galabiose; Distance-dependent dielectric

1. Introduction

The α-D-Gal*p*-(1→4)-β-D-Gal*p* dimer is a component of common plant oligosaccharides known collectively as the α-galactosides. In animals, α-D-galactosidic linkages typically occur at the non-reducing termini of oligosaccharides linked to cell surface lipids or glycoproteins and have been reported as important in infection mechanisms. For example, uropathogenic *Escherichia coli* are known to adhere to uroepithelial cells by their globobiose-binding pili.[1,2] Disaccharides are natural models for the glycosidic linkages in their corresponding homopolysaccharides. The galactose disaccharide globobiose shown in Figure 1 (α-D-Gal*p*-(1→4)-β-D-Gal*p*, also referred to in the literature as galabiose and digalactoside) is thus also of interest as a simple dimer model for the α-(1→4)-linkage in pectic acid, the linear α-(1→4)-D-polygalacturonan, though it lacks a carboxyl group at C5. There is scant experimental evidence on the preferred conformations of either globobiose or polygalacturonan. However, the force response of the pectin polysaccharide has recently been probed by atomic force microscopy (AFM) stretching experiments.[3–5] The two axial bonds in the pectin glycosidic linkage have been postulated to be the source of the unique force extension curve produced by AFM stretching[6] and there has been recent interest in solvent dependence of this molecular elasticity.[4,5]

One of the most straightforward approaches to evaluating the conformational preferences of disaccharides is

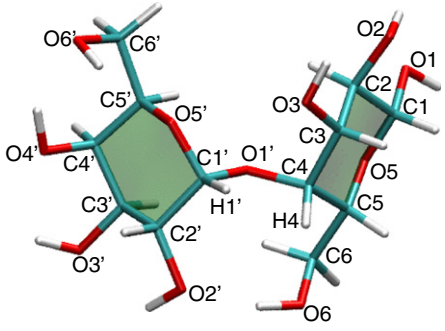

Figure 1. Three-dimensional structure of the globobiose disaccharide, showing the atomic naming scheme.

* Tel.: +27 21 6505107; fax: +27 21 6899465; e-mail: mkuttel@cs.uct.ac.za

0008-6215/$ - see front matter © 2008 Elsevier Ltd. All rights reserved.
doi:10.1016/j.carres.2008.01.038

to investigate the molecular energy as a function of the conformation of the disaccharide linkage. A simple ϕ, ψ Ramachandran plot for a disaccharide gives some insight into preferred conformations and can, with care, be extrapolated to the prediction of polysaccharide structures.[7–11] Relaxed conformational energy maps have been prepared for globobiose and derivatives.[12,13] However, the conformational preferences indicated by these surfaces do not agree with the experimental evidence of a different conformation for globobiose in solution[14] as compared to the solid state.[15] Calculated free energy potential of mean force (PMF) maps are inherently more reliable as they incorporate entropic effects. In addition, if performed in solution, PMF calculations reveal the effect of solvent on a glycosidic linkage. However, PMF calculations in solution are rarely undertaken because of the computational time required to average over all solvent and solute configurations. For example, to date few free energy studies of β-linked galactans[16,17] and none on α-linked galactans have been reported.

Here, four ϕ, ψ PMF surfaces are presented for the globobiose α-(1→4)-linkage in vacuum, explicit solution, using a high dielectric constant and a distance-dependent dielectric coefficient, respectively. These surfaces allow us to locate the global and local minimum energy conformations for globobiose. Further, comparison of the vacuum and explicit solution free energy surfaces provides a quantitative view of the effects of the aqueous solvation on this glycosidic linkage conformation and dynamics. Furthermore, comparison of the dielectric models and the explicit solvation map gives a guide as to how appropriate the use of these simple solvent models are for this disaccharide. This is of particular importance for oligosaccharide AFM simulations, which typically use a dielectric constant to approximate solvent contributions.[4] Though water is known to form solvent bridges between saccharide residues and it has been shown that single-point implicit solvent energies are poor estimators of the free-energy difference of oligosaccharides in solution,[10,11] there have been few attempts[17] to provide a quantitative measure of the difference between the effect of explicit solution and an implicit solvation model on a disaccharide conformation.

2. Computational methods

The glycosidic linkage conformation for globobiose may be defined by the torsion angles, $\phi = \text{H1}'\text{–C1}'\text{–O1}'\text{–C4}$ and $\psi = \text{C1}'\text{–O1}'\text{–C4–H4}$. These definitions for ϕ and ψ are analogous to ϕ_H and ψ_H in IUPAC convention. The β-conformation of globobiose was simulated, as, according to the anomeric ratio for glucose,[18] this is expected to be favoured in solution. Conformations of the globobiose disaccharide were depicted using the VMD visualisation package[19] incorporating a new visualisation algorithm for carbohydrates[20] to highlight the conformation of the glycan rings.

2.1. PMF calculations

Free energy surfaces for globobiose were calculated using a semi-automated adaptive umbrella sampling protocol detailed in prior publications.[21,9] Briefly, the method proceeds as follows.

A series of biased simulations are run, with the applied biasing 'umbrella' potential adapting until it converges to the negative of the PMF surface. The ϕ, ψ umbrella potential for each individual simulation is represented as a $360° \times 360°$ ϕ, ψ grid, with a grid point separation of 2.5°. At each integration step in an umbrella simulation, the specific biasing force to be applied corresponding to the current ϕ, ψ orientation is calculated from a cubic spline of this grid. The first simulation in a series is essentially unbiased, with all grid points in the umbrella surface set to zero. Subsequent simulations use the inverse of the current estimate of the PMF surface as a biasing potential.

Each adaptive umbrella simulation consists of an equilibrium phase of 500 ps, followed by a production phase of 20 ns. A ϕ, ψ distribution histogram is calculated from the production phase of the simulation trajectory. The weighted histogram analysis method (WHAM)[22] is then applied to combine all the trajectory histograms to obtain the current best estimate of the ϕ, ψ PMF surface. Unexplored regions on this PMF surface are set to the maximum energy value of the explored regions (to encourage progression into these regions), and the resultant PMF surface is smoothed. The umbrella potential for the following simulation in the series is set to the negative of this PMF surface and the next iteration is begun. This procedure continues until a series of three successive simulations explore all regions in the ϕ, ψ surface below a predetermined cutoff energy value (typically set at 20 kcal/mol). Using this criterion, approximately 100 simulations are required on average for convergence of the PMF surface, which equates to around 2000 ns simulation time.

2.2. Simulation conditions

All molecular dynamics simulations were performed using the program CHARMM[23] (version 27b1), with modifications incorporated into the USERE module in order to implement both the two-dimensional adaptive umbrella sampling PMF calculations and the stretching simulations. The CSFF carbohydrate parameter set[24] for the CHARMM force field was used to represent the carbohydrate molecules and the TIP3P model was used to represent water.[25]

Two separate PMF calculations were carried out with $\varepsilon_C = 75$. In the first, a dielectric constant was specified using the CHARMM keyword CDIE ($\varepsilon = \varepsilon_C$). In the second, a distance-dependent dielectric coefficient ($\varepsilon = \varepsilon_C r$) was specified using the 'RDIE' CHARMM keyword. Here, approximate solvent screening is achieved by attenuating the electrostatic interaction between two partial charges as they are separated.

For the globobiose explicit solution simulations, the disaccharide was placed in a previously equilibrated cube of 512 TIP3P waters. Solvent water molecules that overlapped with the solute molecule were removed and the system was equilibrated for 500 ps. The solution simulation surrounded the disaccharide with 488 TIP3P water molecules in a cube of length 24.64 Å. The cube was subjected to minimum image periodic boundary conditions to eliminate edge effects.

Initial velocities for the atoms were selected at random from a Boltzmann distribution at 300 K. All simulations were performed in the canonical ensemble (constant n, V, T), using stochastic Langevin dynamics with a frictional coefficient of 62.5 to maintain a constant temperature of 300 K. The equations of motion were integrated using a Leap-Frog Verlet integrator[26] with a step size of 1 fs. The SHAKE algorithm[27] was used to fix the length of bonds involving hydrogen atoms and the water molecule geometry throughout each simulation. Non-bonded interactions were truncated using a switching function applied on a neutral group basis between 10.0 and 12.0 Å. The groups corresponded to electrically neutral collections of atoms in the carbohydrate molecules and entire water molecules for the solvent.

3. Results and discussion

Contour plots of the four PMF surfaces calculated for the globobiose disaccharide under the various solvent conditions appear as shown in Figure 2. The two axial bonds in this α-(1→4)-linkage result in close proximity of the galactose rings and favourable conformations are broadly determined by the small range of orientations that avoid steric clashes. In particular, both the *syn-ϕ/anti-ψ* and the *anti-ϕ/syn-ψ* conformational families suffer from steric crowding between opposing ring hydrogens and hydroxymethyl groups. *syn-ϕ/syn-ψ* Conformations, which separate the primary alcohols

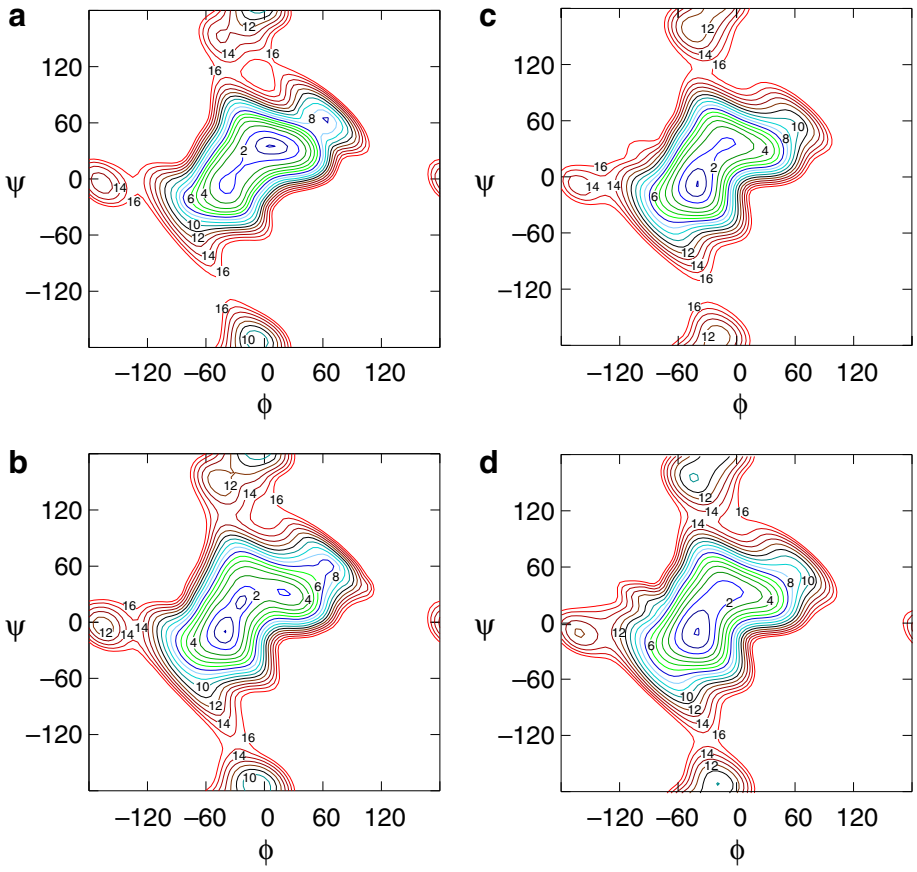

Figure 2. Contour plots of the ϕ, ψ potential of mean force for globobiose using (a) vacuum, (b) explicit TIP3P water, (c) dielectric constant $\varepsilon = 75$ and (d) distance-dependant dielectric $\varepsilon = 75$. Contours are shown at 1 kcal/mol intervals, to a maximum of 16 kcal/mol.

and draw the rings further apart, are therefore favoured for this linkage. These restrictions result in the PMF landscapes all exhibiting the same general features: a broad central *syn*-ϕ/*syn*-ψ valley containing the global energy minimum and one or more additional local minima, a secondary high-energy valley of *syn*-ϕ/*anti*-ψ conformations around ϕ, $\psi = -5°$, 170° and a tertiary *anti*-ϕ/*syn*-ψ valley containing a single minimum in the ϕ, $\psi = -165°$, 5° region.

Globobiose conformations that are favoured in vacuum combine a lack of steric strain with stabilising inter-residue hydrogen bonds, which occur chiefly in the positive ψ region. However, the relative orientation of both rings in globobiose typically prohibits more than one inter-residue hydrogen bond. As an example, the relatively unstrained *syn*-ϕ/*syn*-ψ conformations in the broad global minimum valley are most favoured in the positive ϕ orientations stabilised by a strong O2′–O6 inter-residue hydrogen bond (illustrated in Figure 3a), but the O6′–O3 hydroxyls are too far apart to interact in this conformation. In vacuum, the global *syn*-ϕ/*syn*-ψ minimum conformation occurs at ϕ, $\psi = 5°$, 35°, which represents an optimal O2′–O6 interaction. The additional local minimum in this well at −40°, −5° (Table 1) exhibits an O3–O5′ interaction. These areas correspond to the two principle low-energy regions found in Ramachandran maps of globobiose and eight derivatives[13]. Similarly, for the *syn*-ϕ/*anti*-ψ valley, conformations with ϕ near to zero result in a close O2–O3′ hydrogen bond (Fig. 3b). Thus, in this well the principal local minimum at ϕ, $\psi = -7.5°$, −172.5° (9.1 kcal/mol) is favoured over the local minimum at ϕ, $\psi = -45°$, 150° (12.8 kcal/mol), which pulls these groups further apart. Transitions between the *syn*-ϕ/*anti*-ψ and *syn*-ϕ/*syn*-ψ conformations are disfavoured not only by the high energy difference between the wells ($\Delta G =$ 9.0 kcal/mol, Table 1), but also by a very high energy barrier (15 kcal/mol) to rotation. This high energy barrier should be compared to the much lower energy differences for *syn*-ψ to *anti*-ψ transitions in the α-(1→4)-linked maltose disaccharide ($\Delta G = 2.3$ kcal/mol),[9] as it indicates that this type of conformational transition is much less likely to be important to the dynamics of galactan α-(1→4)-linkages than it is for α-(1→4)-linked glucans.

Inter-residue hydrogen bonds can also be seen to stabilise more sterically strained conformations in vacuum: the small local minimum feature at ϕ, $\psi = 60°$, 60° is a result of a stabilising O2–O3′ hydrogen bond (Fig. 3d). Further, the strained tertiary *anti*-ϕ/*syn*-ψ valley brings H4 into close proximity with H5′ and H3′ on the sister ring, but unusually allows for two stabilising inter-residue bonds at once, between O2–O3′ and O6–O6′.

As was previously found for maltose,[9] solvation of globobiose with explicit water has the principal effect

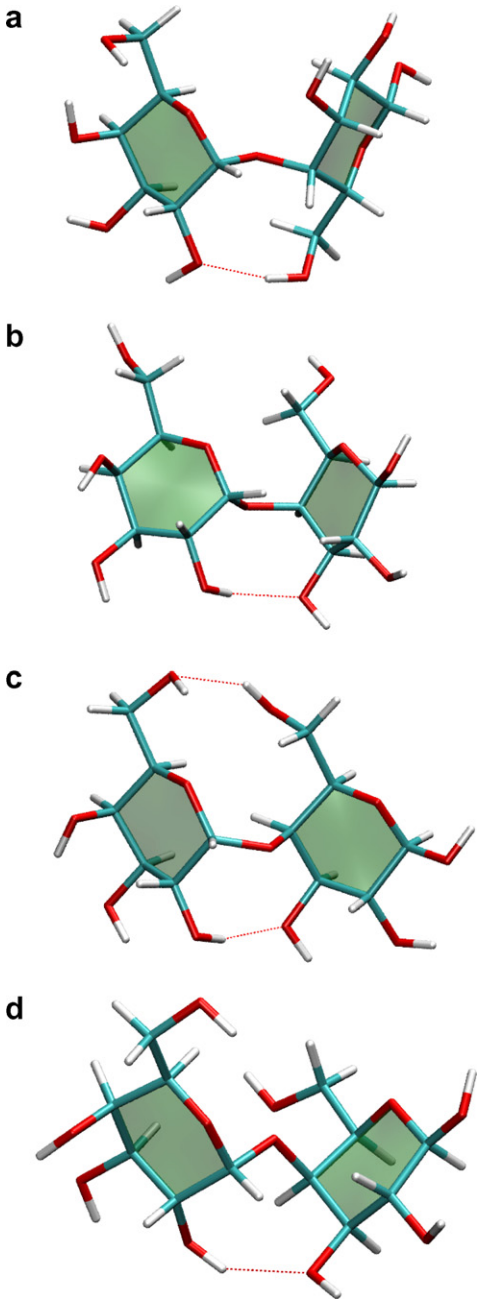

Figure 3. Globobiose structures in vacuum, showing inter-residue hydrogen bonds. (a) *syn*-ϕ/*syn*-ψ Global energy minimum conformation: ϕ, $\psi = 8°$, 35°. (b) *syn*-ϕ/*anti*-ψ Conformation: ϕ, $\psi = -5°$, −177°. (c) *anti*-ϕ/*syn*-ψ Conformation: ϕ, $\psi = -164°$, −6°. (d) Strained *syn*-ϕ/*syn*-ψ conformation with ϕ, $\psi = 60°$, 60°, showing the stabilising O2–O3′ bond.

of extending the range of the stabilising inter-residue hydrogen bonds with bridging water molecules. Ab initio studies have shown that intermolecular hydrogen bonds to water molecules bridging the rings are of similar strength to, and hence competitive with, intramolecular hydrogen bonds (at around 4.5 kcal/mol for maltose).[28] Structures with bridging inter-residue hydrogen bonds with water intermediaries are expected to be

Table 1. Values of the ϕ, ψ dihedral angles in degrees for local minima and transition barrier regions on the four ϕ, ψ PMF surfaces for globobiose

	Conformational region							
	syn-ϕ/*syn*-ψ		*syn*-ϕ/*anti*-ψ		*anti*-ϕ/*syn*-ψ		barrier regions	
	ϕ, ψ	ΔG	ϕ, ψ	ΔG	ϕ, ψ	ΔG	ϕ, ψ	ΔG
Vacuum	5, 35	(0)	−7.5, −172.5	(9.1)	−165, −5	(12.5)	−40, 115	(15.4)
	−40, −5	(1.6)	−45, 150	(12.8)			−132.5, −7.5	(15.7)
TIP3P	−40, −10	(0)	−7.5, −172.5	(9.0)	−165, −5	(11.3)	−40, 115	(13.7)
	−25, 20	(0.5)	−45, 150	(11.2)			−132.5, −10	(14.7)
	20, 30	(1.1)						
CDIE	−42.5, −7.5	(0)	−20, −170	(11.3)	−162.5, −10	(13.3)	40, 115	(15.8)
$\varepsilon = 75$	−10, 35	(1.9)	−45, 155	(11.2)			−132.5, −10	(14.7)
RDIE	−42.5, −7.5	(0)	−20, −170	(10.0)	−162.5, −10	(11.8)	40, 115	(14.4)
$\varepsilon = 75$			−45, 155	(9.9)			−132.5, −10	(13.2)

Approximate free energy values (in kcal/mol) relative to the global energy minimum are quoted in brackets.

entropically favoured because of the variety of possible hydrogen bonding arrangements that can occur with the water molecules. For globobiose, this results in a shift of the global minimum structure to ϕ, $\psi = -40°$, $-7.5°$, which is close to the ϕ, $\psi = -39°$, $-15°$ solution conformation calculated from NMR–NOE data for globobiose.[14] Two additional local minima appear in the global *syn*-ϕ/*syn*-ψ well at ϕ, $\psi = -25°$, $20°$ (0.5 kcal/mol) and ϕ, $\psi = 20°$, $30°$ (1.1 kcal/mol, Table 1). These local minima represent structures ideally oriented for water bridges, as illustrated by the conformations in Figure 4a–c. The ϕ, $\psi = -25°$, $20°$ minimum is close to the X-ray crystal structure values of ϕ, $\psi = -18°$, $35°$ and also exhibits the O3–O5′ interaction seen in the crystal structure.[13]

The relative energy and location of the secondary minimum for globobiose remains effectively unchanged at ϕ, $\psi = -7.5°$, $-175°$ ($\Delta G = 9.0$ kcal/mol). Though the secondary well is broadened slightly by bridging water hydrogen bonds between the O6–O6′ and O2–O3′ hydroxyls, respectively, the range of this valley is still principally limited by steric clashes. However, the barrier height for transitions between *syn*-ϕ/*syn*-ψ and the secondary *syn*-ϕ/*anti*-ψ well is lowered by 2 kcal/mol in explicit solution for a positive ψ rotation (Table 1). A similar mechanism lowers the corresponding region of the maltose solution PMF by 2 kcal/mol.[9] Transition to the *syn*-ϕ/*anti*-ψ conformations requires breaking the close inter-residue O1–O6′ hydrogen bond, which forms in this region. In solution, bridging water molecules lessen this energetic penalty. In addition, the relative orientation of the rings in this conformation results in a close fit of the saccharide hydroxyls with the hydrogen-bonding network in aqueous solution and hence facilitates the formation of many-atom water bridges between the saccharide hydroxyls. The fact that the barrier height to rotation between the primary and secondary valleys is not lowered significantly in the high dielectric map (Fig. 2c) as compared to vacuum indicates that the lowering in energy is indeed an effect of the unique properties of the aqueous environment.

Bridging waters extend the range of inter-residue hydrogen bonds in other regions of the PMF maps as well, as is shown by the associated broadening of the local energy minima at both ϕ, $\psi = 60°$, $60°$ and the area around ϕ, $\psi = -40°$, $160°$. In contrast, the location and size of the tertiary *anti*-ϕ/*syn*-ψ minimum at ϕ, $\psi = -165°$, $5°$ is unchanged in explicit solution, with the energy reduced slightly by 1 kcal/mol. The ranges of the internal O2–O3′ and O6–O6′ hydrogen bonds in this conformation are limited by steric clashes.

The PMF surfaces produced by the high dielectric constant and distance-dependent dielectric protocols are quite similar, as is to be expected for a small molecule. The principle difference between these maps is the relative energy of the secondary and tertiary minimum wells, which are raised by approximately 2 kcal/mol in the constant dielectric model relative to the distance-dependent dielectric. The shielding effect of the large dielectric constant used in both these models has the result of discounting the energy gain from relatively long-distance inter-residue electrostatic interactions. However, the distance-dependent dielectric model will favour close-range electrostatic interactions. For the explicit and implicit solvent models, the chief change in the free energy surface in comparison to vacuum is a relative disfavouring of the region extending from ϕ, $\psi = -30°$, $-30°$ to ϕ, $\psi = 60°$, $60°$ and a shift of the preferred conformations to more negative ψ values in the central *syn*-ϕ/*syn*-ψ valley. For global minimum *syn*-ϕ/*syn*-ψ conformations of globobiose, both the use of a large dielectric constant (Fig. 2c) and the distance-dependent dielectric coefficient (Fig. 2d) have a similar effect to explicit solvation: the global minimum shifts to ϕ, $\psi = -45°$, $-10°$ (Fig. 5a), close to the water minimum. This effect may be taken as confirmation that, in the absence of favourable hydrogen conformations, this is the region of the map with least steric strain. Either

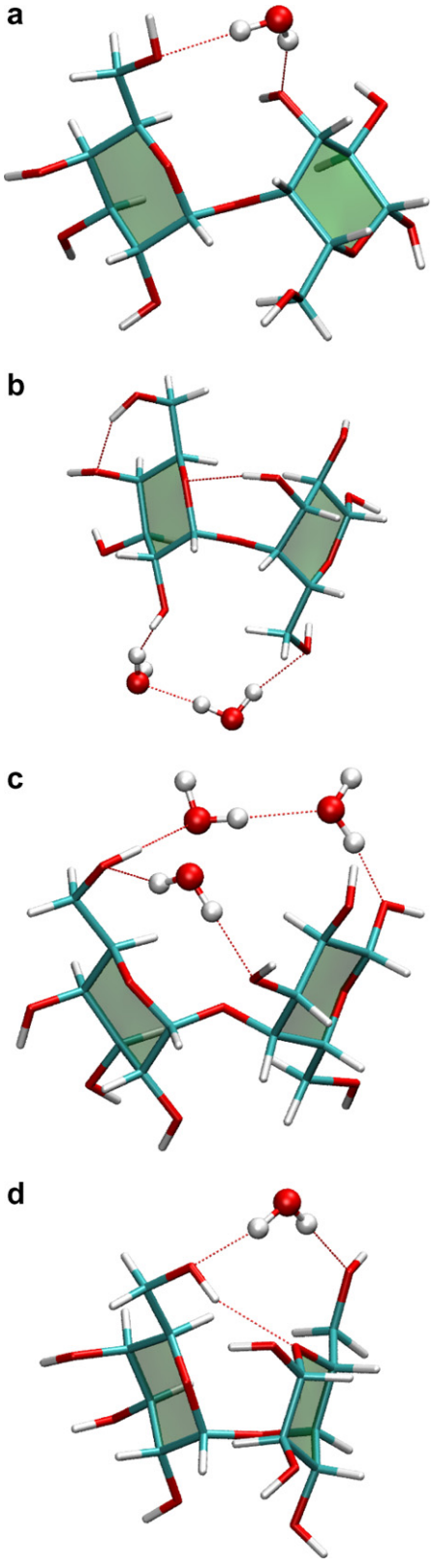

Figure 4. Globobiose structures in water showing bridging water hydrogen bonds. (a) *syn*-ϕ/*syn*-ψ Global energy minimum conformation: ϕ, $\psi = -40°$, $-15°$. (b) *syn*-ϕ/*syn*-ψ Local minimum conformation: ϕ, $\psi = -22°$, 26°. (c) *syn*-ϕ/*syn*-ψ Local minimum conformation: ϕ, $\psi = 21°$, 31°. (d) *syn*-ϕ/*anti*-ψ conformation, ϕ, $\psi = -60°$, $-159°$, showing a water bridge and O5 H-bond stabilising this otherwise unfavourable conformation.

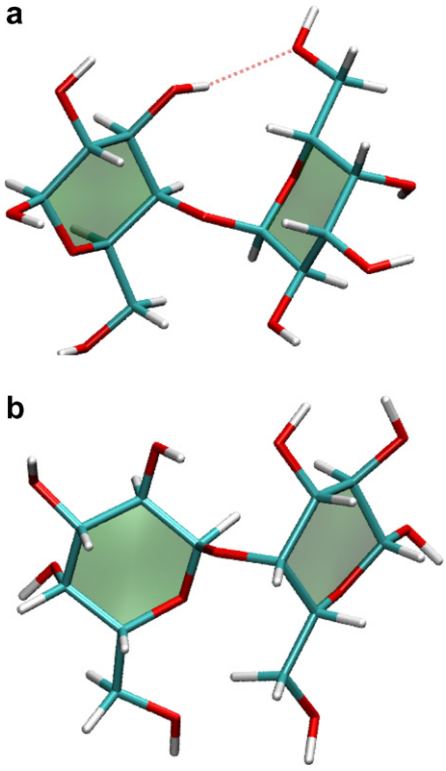

Figure 5. Globobiose structures using a distance-dependent dielectric coefficient. (a) *syn*-ϕ/*syn*-ψ Global minimum structure: ϕ, $\psi = -44°$, $-11°$. (b) *syn*-ϕ/*anti*-ψ Secondary minimum structure: ϕ, $\psi = -40°$, 159°.

discounting the internal hydrogen bonds or extending them via water intermediaries has the same effect in that it allows the least sterically strained structures to predominate. The overall shape and region of the *syn*-ϕ/*syn*-ψ global minimum valley is also similar to that in water. Therefore, the use of either of these simple solvent models is expected to be sufficient for the simple reproduction of the globobiose global energy minimum structure. This result is in agreement with PMF studies of neocarabiose, where the use of the CHEAT95 force field,[29] which attenuates hydrogen-bonding interactions, reproduced the location of the global energy minimum.[17]

However, aside from the global minimum, the use of both the dielectric models has a marked effect on the location and relative energies of the other local minima in the PMF maps. In the distance-dependent dielectric model PMF shown in Figure 2d, the central *syn*-ϕ/*syn*-ψ well is markedly broader than in the vacuum and explicit solution and contains just the single global minimum: compare the 2 kcal/mol contour shown in Figure 2b and c, respectively. For the high dielectric constant map shown in Figure 2c, the local minimum at ϕ, $\psi = -10°$, 35° has no counterpart in either the water or the vacuum map. Thus, the dynamic behaviour and population distribution of the globobiose disaccha-

ride when using either of these two models are not expected to be a representative of the aqueous environment, where dynamics are expected to be more restricted. This tallies with prior simulations of maltose, as well as with results for β-linked agarose chains, where dynamics were more restricted in water than when using a bulk dielectric model.[30] Further, these PMF maps differ more markedly from solution in the secondary *syn*-ϕ/*anti*-ψ well. Here, both maps show a shift of the local minimum to ϕ, $\psi = -45°$, 155° and the local energy minimum for the constant dielectric map is 2 kcal/mol higher in energy than the water PMF. In these conformations, inter-residue hydrogen bonds compete against more sterically favourable arrangements. In addition, the barrier heights to rotation are higher than in the aqueous case. However, this is not a large margin for an already very unfavoured transition to a high-energy conformation that is unlikely to have much significance for either the disaccharide or the α-(1→4)-linked galactans. Conformations with ϕ, $\psi = -7.5°$, $-175°$ extrapolated to oligosaccharide structures lead to cyclic galactans analogous to the cyclodextrins for amylose. However, these hypothetical structures are likely to be highly strained, with 5 units per cycle. Further, the ϕ, $\psi = -45°$, 155° local minimum in the high dielectric PMFs corresponds to a very tight helix with 4 galactose units per turn. Therefore, an assumption that α-galactan (and by extension polygalacturonan) structure and dynamics occur chiefly within the *syn*-ϕ/*syn*-ψ well is likely to be valid.

4. Conclusions and future work

These PMF studies provide a thorough characterisation of the α-(1→4)-linkage in globobiose. The linkage is shown to be constrained, with only a small range of *syn*-ϕ/*syn*-ψ conformations accessible at standard temperature and pressure. Due to high energy differences and even higher barriers to rotation, *syn*-ϕ/*syn*-ψ to *syn*-ϕ/*anti*-ψ transitions are unlikely to be a feature of the dynamics of α-galactosides and polygalacturonan polysaccharides. In addition, the use of either a high dielectric constant or a distance-dependent dielectric coefficient is shown to achieve the same principal effect as explicit solvation on the globobiose molecule, which is to shift the preferred conformation from ϕ, $\psi = 5°$, 35° to ϕ, $\psi = -40°$, $-7.5°$. Differences between the explicit and implicit solution maps are primarily restricted to areas of little relevance to oligosaccharides. This leads to the conclusion that the use of a distance-dependent dielectric as a substitute for explicit solvent, while not reproducing all the features of the dynamic behaviour of globobiose, is likely to be a satisfactory approximation for the simulations of α-galactan oligosaccharides. Future work will extend to corroborative studies of the chain dynamics for α-galactoside and polygalacturonan oligosaccharides.

Acknowledgement

The author thanks the South African National Bioinformatics Network for financial support.

References

1. Lund, B.; Lindberg, F.; Marklund, B.-I.; Normark, S. *Proc. Natl. Acad. Sci. U.S.A.* **1987**, *84*, 5898–5902.
2. Hultgren, S. J.; Abraham, S. N.; Caparon, M.; Falk, P.; St. Geme, J. W., III; Normark, S. *Cell* **1993**, *73*, 887–901.
3. Marszalek, P. E.; Pang, Y.-P.; Li, H.; Yazal, Y. E.; Oberhauser, A. F.; Fernandez, J. M. *Proc. Natl. Acad. Sci. U.S.A.* **1999**, *96*, 7894–7898.
4. Zhang, Q.; Marszalek, P. E. *Polymer* **2006**, *47*, 2526–2532.
5. Williams, M. A. K.; Marshall, A. T.; Anjukandi, P.; Haverkamp, R. G. *Phys. Rev. E* **2007**, *76*, 021927.
6. Zhang, Q.; Marszalek, P. E. *J. Am. Chem. Soc.* **2006**, *128*, 5596–5597.
7. Brant, D. A.; Dimpfl, W. L. *Macromolecules* **1970**, *3*, 655–665.
8. Brant, D. A. *Pure Appl. Chem.* **1997**, *69*, 1885–1892.
9. Kuttel, M. M.; Naidoo, K. J. *J. Phys. Chem. B* **2005**, *109*, 7468–7474.
10. Xia, J.; Daly, R. P.; Chuang, F.-C.; Parker, L.; Jensen, J. H.; Margulis, C. J. *J. Chem. Theory Comput.* **2007**, *3*, 1620–1628.
11. Xia, J.; Daly, R. P.; Chuang, F.-C.; Parker, L.; Jensen, J. H.; Margulis, C. J. *J. Chem. Theory Comput.* **2007**, *3*, 1629–1643.
12. Perico, A.; Mormino, M.; Urbani, R.; Cesàro, A.; Tylianakis, E.; Dais, P.; Brant, D. A. *J. Phys. Chem. B* **1999**, *103*, 8162–8171.
13. Gouvion, C.; Mazeau, K.; Tvaroska, I. *J. Molec. Struct. (Theochem)* **1995**, *344*, 157–170.
14. Frejd, K. B. T.; Kihlberg, J.; Magnusson, G. *Carbohydr. Res.* **1988**, *176*, 253.
15. Svensson, G.; Albertsson, J.; Svensson, C. *Carbohydr. Res.* **1986**, *146*, 29–38.
16. Stortz, C. A. *Carbohydr. Res.* **2002**, *337*, 2311–2323.
17. Ueda, K.; Brady, J. W. *Carbohydr. Res.* **2004**, *339*, 1953–1960.
18. Angyal, S. J. *Aust. J. Chem.* **1968**, *21*, 2737–2746.
19. Humphrey, W.; Dalke, A.; Schulten, K. *J. Mol. Graphics* **1996**, *14*, 33–38.
20. Kuttel, M.; Gain, J.; Burger, A.; Eborn, I. *J. Mol. Graphics Modell.* **2006**, *25*, 380–388.
21. Kuttel, M. M. *Carbohydrate Conformational Dynamics and Thermodynamics*, Thesis, University of Cape Town, 2003.
22. Kumar, S.; Bouzida, D.; Swendsen, R. H.; Kollman, P. A.; Rosenberg, J. M. *J. Comput. Chem.* **1992**, *13*, 1011–1021.
23. Brooks, B. R.; Bruccoleri, R. E.; Olafson, B. D.; States, D. J.; Swaminathan, S.; Karplus, M. *J. Comput. Chem.* **1983**, *4*, 187–217.
24. Kuttel, M.; Brady, J. W.; Naidoo, K. J. *J. Comput. Chem.* **2002**, *23*, 1236–1243.

25. Jorgensen, W. L.; Chandrasekhar, J.; Madura, J. D.; Impey, R. W.; Klein, M. L. *J. Chem. Phys.* **1983**, *79*, 926–935.
26. Hockney, R. W. *Meth. Comput. Phys.* **1970**, *9*, 136–211.
27. Ryckaert, J. P.; Ciccotti, G.; Berendsen, H. J. C. *J. Comput. Phys.* **1977**, *23*, 327–341.
28. Naidoo, K. J.; Chen, Y.-J. *Mol. Phys.* **2003**, *101*, 2687–2694.
29. Kouwijzer, M. L. C. E.; Grootenhuis, P. D. J. *J. Phys. Chem.* **1995**, *99*, 13426–13436.
30. Haggett, N. M. W.; Hoffmann, R. A.; Howlin, B. J.; Webb, G. A. *J. Mol. Model.* **1997**, *3*, 301–310.